

Research Paper

Weakly singular BIEM for analysis of cracks embedded in symmetric elastic whole space

T.N. Pham¹, J. Rungamornrat², W. Pansuk³, Y. Sato⁴

ARTICLE INFORMATION

Article history:

Received: 03 January, 2017

Received in revised form: 21 March, 2017

Accepted: 21 July, 2017

Publish on: 07 September, 2018

Keywords:

Anisotropy

BIEMs

Cracks

Elastic whole space

Weakly singular

ABSTRACT

In this paper, a weakly singular boundary integral equation method is developed for the stress analysis of an anisotropic, linearly elastic, cracked whole space possessing a plane of symmetry. This study should offer an alternative powerful tool essential for the modeling of both near-surface and deeply embedded defects in a rock/soil medium. A system of governing equations is established using a pair of weakly singular, weak-form, displacement and traction integral equations for the cracked whole space along with the symmetric condition. The final equations contain only unknown crack-face data in a lower-half of the whole space. In addition to their capability to treat cracks of arbitrary shape, material anisotropy and general loading conditions, all involved kernels are only weakly singular allowing all integrals to be interpreted in the sense of Riemann sum. A symmetric Galerkin boundary element method together with the Galerkin approximation is implemented to solve the governing integral equations for the unknown crack-face data. To further enhance the accuracy and efficiency of the proposed scheme, special basis functions are introduced to approximate the near-front field and the interpolation technique is adopted to evaluate all kernels for generally anisotropic materials. The solved crack-face displacement data is then utilized to post-process for the essential fracture information along the crack front. Various scenarios are employed to verify the proposed technique and a selected set of results is presented to demonstrate its accuracy and computational robustness.

1. Introduction

Modeling and analysis of a medium containing pre-existing damages and flaws (e.g., dislocations and cracks) has been found an essential procedure in the fracture-based failure/fatigue assessment. There are

various situations encountered in practices when damages and flaws are located in a region relatively near the boundary or deeply inside the body and, in addition, their sizes are comparatively small in comparison with the characteristic length scale of the body; for instance, the modeling of near-surface/deep fractures in a large scale

¹ PhD Student, Applied Mechanics and Structures Research Unit, Department of Civil Engineering, Faculty of Engineering, Chulalongkorn University, Bangkok, THAILAND, phamngoctien@muce.edu.vn

² Corresponding Author, Associate Professor, Applied Mechanics and Structures Research Unit, Department of Civil Engineering, Faculty of Engineering, Chulalongkorn University, Bangkok, THAILAND, jaron.r@chula.ac.th

³ Associate Professor, Innovative Construction Materials Research Unit, Department of Civil Engineering, Faculty of Engineering, Chulalongkorn University, Bangkok, THAILAND, withit.p@chula.ac.th

⁴ Associate Professor, Department of Civil Engineering, Faculty of Engineering, Hokkaido University, Sapporo, JAPAN, ysato@eng.hokudai.ac.jp

Note: Discussion on this paper is open until March 2019

rock and soil medium and simulations of hydraulically induced cracks deeply beneath the ground used in the production enhancement of natural oil and gas (e.g., Mendelsohn, 1984a; Mendelsohn, 1984b; Yew, 1997). To simplify the modeling of those physical problems, a half space or whole space together with a selected set of governing physics (e.g., a theory of linear elasticity and linear elastic fracture mechanics) is commonly used to describe the response of such large scale cracked body. The influence of the remote boundary on the local response of interest is generally insignificant and can, therefore, be discarded in the modeling without loss of accuracy of predicted results. To perform the full analysis of such simplified mathematical model, the solution procedure plays a crucial role in both the accuracy and computational efficiency and it must be properly chosen to suit each involved scenario.

Various analytical techniques such as methods of integral transform, representation theories, and potential functions have been proposed and used extensively to solve various types of boundary value problems with semi-infinite and infinite domains (e.g., Srivastava and Singh, 1969; Mayrhofer and Fischer, 1989; Wang, 2004; Chen and Shioya, 2000). However, their applications are quite limited to either two-dimensional problems or three-dimensional cases with extremely idealized settings. Such limitation becomes more apparent when the complexity of involved physical phenomena increases (e.g., material constitutive laws, presence of singularities, and general boundary and loading conditions). To enhance the modeling capability, a variety of numerical procedures have been continuously developed to solve half-space and whole-space problems. Standard finite element methods (FEMs) have been well-established in the past several decades (Oden and Carey, 1984; Zienkiewicz and Taylor, 2000; Hughes, 2000) and successfully applied to solve numerous problems in various disciplines. It is worth noting, however, that when applied to treat problems involving unbounded domains, the computational efficiency of FEMs can be significantly degraded. For instance, a standard discretization procedure cannot be directly applied to infinite and semi-infinite domains. A domain truncation together with a set of proper remote boundary conditions is commonly employed to establish an approximate domain of finite dimensions prior to the discretization. Another limited capability of standard FEMs is apparent when they are applied to solve fracture-related problems. In the analysis, substantially fine meshes are required in a region surrounding the discontinuities in order to accurately capture the complex field and extract essential local fracture information along the crack front (Swenson and Ingraffea, 1988; Martha et al., 1993; Ayhan et al., 2003).

Boundary integral equation methods (BIEMs) have been also well-recognized as one of the most efficient numerical techniques for modeling linear boundary value problems (e.g., Brebbia and Dominguez, 1989; Cruse, 1988; Liggett and Liu, 1983). Efficiency of BIEMs over standard FEMs becomes more apparent when a domain to be treated is unbounded (e.g., Gu and Yew, 1988; Xu and Ortiz, 1993; Xu, 2000; Rungamornrat and Wheeler, 2006; Rungamornrat and Mear, 2008b; Rungamornrat et al., 2015), the ratio between the domain-measure and the boundary-measure is large, and the domain contains an embedded singularity such as dislocations and cracks (Rungamornrat and Mear, 2008b; Rungamornrat et al., 2015; Saez et al., 1997; Li et al., 1998; Frangi et al., 2002; Ariza and Dominguez, 2004; Rungamornrat, 2006). This is due to the key nature of the governing integral equation underlying the methods; for a domain that is homogeneous and free of distributed source, the governing equation involves only integrals over the boundary of the domain and the surface of discontinuity. Besides those desirable features, BIEMs still possess a major drawback associated with the treatment of singularity induced by kernels present in the governing integral equations. For conventional BIEMs, involved strongly singular and hyper-singular kernels often pose theoretical and numerical difficulties including the existence and interpretation of singular integrals (e.g., Martin and Rizzo, 1996; Chen, 2003a), issues associated with the smoothness requirement of boundary data (e.g., Martin and Rizzo, 1996), and the requirement of significant computational cost and special numerical quadrature to evaluate involved integrals (e.g., Gray et al., 1990; Martha et al., 1992; Ariza et al., 1997; Chen, 2003b; Qin and Noda, 2004; Zhao et al., 2004). To circumvent such drawback, the BIEMs based on a set of singularity-reduced integral equations are commonly employed.

Regularized BIEMs have been continuously developed for past several decades and the historical background and current advances relevant to the present study can be briefly summarized below. Bui (1977) and Weaver (1977) independently developed the singularity-reduced traction integral equations for isolated planar cracks in an isotropic, elastic whole space under pure mode-I loading conditions. The extension to treat material anisotropy was carried out later by Sladek and Sladek (1982). While the strength of singularity was reduced from hypersingular to strongly singular, the regularization was still incomplete in the sense that the validity of involved integrals still requires the derivative of the relative crack-face displacement to be continuous. Within the context of fracture analysis in linear elastic media, development of the weakly singular boundary integral equations has

been well-established. Gu and Yew (1988) was able to develop the first weakly singular boundary integral equation for the traction. While the derived integral equation is completely regularized, the development is restricted to an isotropic elastic whole space and a planar crack under the pure mode-I loading condition. Xu and Ortiz (1993) applied results from the dislocation theory to develop the weakly-singular, weak-form traction boundary integral equation for modeling isolated cracks of arbitrary shapes in an isotropic elastic, whole space. Later, Bonnet (1995) exploited the integration-by-parts technique together with certain representations of fundamental solutions to establish a pair of weakly singular displacement and traction integral equations for modeling isotropic, linearly elastic, uncracked finite bodies. Li (1996) developed a regularization procedure to derive the weakly singular integral equations for modeling cracks of arbitrary shapes in both isotropic, linearly elastic, whole space and half-space. Li et al. (1998) extended the work of Li (1996) to derive the weakly singular, weak-form integral equations for both the displacement and traction and successfully implemented the symmetric Galerkin boundary element method to solve cracks in isotropic, finite bodies. Later, Rungamornrat and Mear (2008a) proposed a systematic regularization technique to develop a complete set of singularity-reduced integral relations for both dislocations and cracks in generally anisotropic elastic media. While a vast amount of researches concerning the development of weakly singular BIEMs for cracks in unbounded elastic media has been well established, most of existing investigations are restricted only to the derivation of traction integral equation for cracks and the determination of stress intensity factors. The analysis for the nonsingular terms such as the T-stress along the crack front has not been recognized. In addition, the integration of existing symmetry to enhance the computational efficiency and the treatment of material

anisotropy for cracks in an elastic half-space under symmetric boundary conditions has not been found.

In the present study, a systematic regularization technique proposed by Rungamornrat and Mear (2008a) is extended to establish a set of singularity-reduced boundary integral equations for either a cracked elastic whole space containing a plane of symmetry or a cracked elastic half-space subjected to a symmetric condition on the free surface. The development is carried out in a general framework allowing the treatment of material anisotropy, cracks of arbitrary shapes, and general crack-face loading. The resulting weakly singular, weak-form boundary integral equations for both the displacement and traction are then employed as the basis in the implementation of the weakly singular, symmetric Galerkin boundary element method for solving unknown crack-face data and post-processing for essential fracture information. Remaining sections of this paper are organized to incorporate the clear problem description, the development of regularized boundary integral equations, the solution procedure, results and discussion, and conclusions and remarks.

2. Problem description

Consider an elastic cracked whole space Ω that possesses a plane of symmetry as shown schematically in **Fig. 1(a)**. A reference Cartesian coordinate system $\{O; x_1, x_2, x_3\}$ with a set of orthonormal base vectors $\{e_1, e_2, e_3\}$ used in the present development is chosen such that the origin O is located on the plane of symmetry; the x_3 -axis directs downward normal to the plane of symmetry; and the x_1 - and x_2 - axes follow the right hand rule. The medium is made of a homogeneous, anisotropic, linearly elastic material with $x_3 = 0$ being the plane of material symmetry. The cracks in the undeformed state are represented by two geometrically identical, piecewise smooth surfaces S_c^+ and S_c^- with the

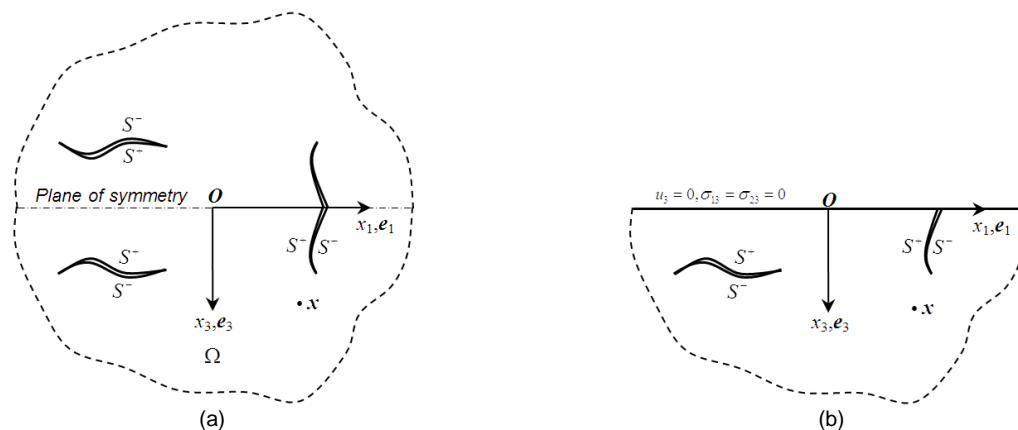


Fig. 1. Schematic of **(a)** cracked whole space with $x_3 = 0$ as plane of symmetry and **(b)** equivalent cracked half-space with symmetric conditions on free surface.

outward unit normal vectors n^+ and n^- , respectively. In the present study, it is assumed that the body force and remote loading are absent and the medium is loaded by self-equilibrated tractions on the crack surfaces. It is worth noting that the influence of the body force and remote loading condition can be readily treated via the superposition technique together with an uncracked state. In addition to an elastic field induced within the cracked medium due to applied loadings, the essential fracture data such as the relative crack-face displacement, the stress intensity factors, and the T-stress components along the crack front are of primary interest.

From the symmetry of all prescribed data, it can be verified that an elastic field of a lower-half of the cracked whole space shown in **Fig. 1(a)** is identical to that of a half-space containing the same crack and subjected to symmetric boundary conditions on the free surface (i.e., the displacement normal to the free surface u_3 and shear tractions σ_{13}, σ_{23} vanish) as indicated in **Fig. 1(b)**. As a result, it is sufficient to solve the equivalent cracked half-space and then exploit the symmetry to obtain the complete solution of the cracked whole space. Using such reduced domain in the simulations clearly reduces the number of degrees of freedom approximately by half.

3. Formulation of governing equations

This section presents the development of a set of completely regularized boundary integral equations for the cracked whole space possessing a plane of symmetry shown in **Fig. 1(a)**. The derivation is carried out only for the lower-half of the domain or, equivalently, for the equivalent cracked half-space shown in **Fig. 1(b)**. First, the displacement and stress fundamental solutions for an uncracked half-space subjected to the symmetric condition on the free surface are constructed and such results are then utilized to form a pair of boundary

integral relations for the displacement and stress of the equivalent cracked half-space. Finally, a systematic regularization technique based on the integration by parts via Stokes' theorem is adopted to establish a set of singularity-reduced boundary integral equations. Special representations of involved kernels essential for assisting such regularization procedure are also provided in details.

3.1 Fundamental solutions for uncracked half-space under symmetric conditions

To construct the fundamental solutions for the displacement and stress of an uncracked half-space subjected to symmetric boundary conditions on the surface $x_3 = 0$, the existing fundamental solutions of an elastic whole space (Ting and Lee, 1997; Wang, 1997) can be employed together with the symmetry as described below.

Now, consider the equivalent uncracked half-space subjected to symmetric boundary conditions and a unit concentrated force $\delta_{ip}e_i$ at a source point $x = x_k e_k$ as illustrated in **Fig. 2(b)** where δ_{ip} denotes the Kronecker-delta symbol. Here and in what follows, standard indicial notation and Einstein summation convention apply. It is apparent that the considered half-space is identical to the lower half of a uncracked whole space subjected to a unit concentrated force $\delta_{ip}e_i$ at a point $x = x_k e_k$ and a unit concentrated force $\bar{\delta}_{ip}e_i$ at the image point $\bar{x} = \bar{x}_k e_k$ as illustrated in **Fig. 2(a)** where $\bar{x}_k = \bar{\delta}_{kp} x_p$ and $\bar{\delta}_{ip}$ are defined by $\bar{\delta}_{11} = \bar{\delta}_{22} = -\bar{\delta}_{33} = 1$ and $\bar{\delta}_{ij} = 0$ for $i \neq j$. The symmetric boundary conditions (i.e., $u_3 = 0$ and $\sigma_{13} = \sigma_{23} = 0$) are automatically satisfied along the plane $x_3 = 0$ of the whole space for the given applied loads. Upon employing this correspondence together with the superposition of the whole space fundamental solutions, the fundamental solutions for the displacement and stress of the uncracked half-space under the symmetric boundary conditions, denoted respectively by $\bar{U}_j^p(\xi, x)$ and $\bar{S}_{ij}^p(\xi, x)$,

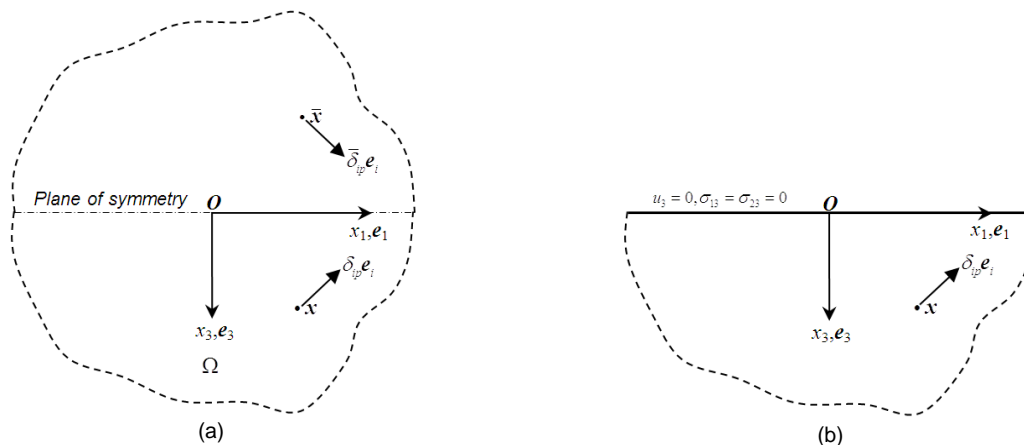


Fig. 2. Schematics of **(a)** uncracked whole space under unit concentrated force $\delta_{ip}e_i$ at x and unit concentrated force $\bar{\delta}_{ip}e_i$ at image point \bar{x} and **(b)** uncracked half-space under symmetric boundary conditions on $x_3 = 0$ and unit concentrated force $\delta_{ip}e_i$ at x .

can be obtained as

$$\bar{U}_j^p(\xi, \mathbf{x}) = U_j^p(\xi - \mathbf{x}) + \bar{\delta}_{pk} U_j^k(\xi - \bar{\mathbf{x}}) \quad [1]$$

$$\bar{S}_{ij}^p(\xi, \mathbf{x}) = S_{ij}^p(\xi - \mathbf{x}) + \bar{\delta}_{pk} S_{ij}^k(\xi - \bar{\mathbf{x}}) \quad [2]$$

where $U_j^p(\xi - \mathbf{x})$ and $S_{ij}^p(\xi - \mathbf{x})$ are the displacement and stress fundamental solutions of an uncracked whole space under a unit concentrated force $\delta_{ij}e_i$ at a source point $\mathbf{x} = x_k e_k$. The explicit form of $U_j^p(\xi - \mathbf{x})$ and $S_{ij}^p(\xi - \mathbf{x})$ can be found in the work of Rungamornrat and Mear (2008a), Ting and Lee (1997), and Wang (1997). From the structure of $U_j^p(\xi - \mathbf{x})$ and $S_{ij}^p(\xi - \mathbf{x})$ together with [1] and [2], it can be concluded that $\bar{U}_j^p(\xi, \mathbf{x})$ and $\bar{S}_{ij}^p(\xi, \mathbf{x})$ are singular only at a single point $\xi = \mathbf{x}$ within the half-space of $\mathcal{O}(1/r)$ and $\mathcal{O}(1/r^2)$, respectively, where $r = \|\xi - \mathbf{x}\|$.

3.2 Standard integral relations for equivalent cracked half-space

By applying the reciprocal theorem to the equivalent cracked half-space shown in **Fig. 1(b)** along with the elastic state associated with a fundamental problem of an uncracked half-space shown in **Fig. 2(b)**, it yields an integral relation for the displacement at any interior point \mathbf{x} of the equivalent cracked half-space as

$$u_p(\mathbf{x}) = \int_{S_c^+} \bar{U}_j^p(\xi, \mathbf{x}) \Sigma t_j(\xi) dA(\xi) - \int_{S_c^-} \bar{S}_{ij}^p(\xi, \mathbf{x}) n_i^+(\xi) \Delta u_j(\xi) dA(\xi) \quad [3]$$

where $\Sigma t_j(\xi) = t_j(\xi^+) + t_j(\xi^-)$ denotes the sum of the prescribed crack-face traction; $\Delta u_j(\xi) = u_j(\xi^+) - u_j(\xi^-)$ denotes the jump in the unknown crack-face displacement; and $\xi^+ \in S_c^+$ and $\xi^- \in S_c^-$ are two coincident points on the crack surface. It should be remarked that the reduction to integrals over a single crack surface S_c^+ stems directly from the continuity of the fundamental solutions $\bar{U}_j^p(\xi, \mathbf{x})$ and $\bar{S}_{ij}^p(\xi, \mathbf{x})$ at any field point ξ . By first taking the derivative of [3] to obtain the spatial gradient of $u_p(\mathbf{x})$ with respect to x_i and then employing the constitutive law for linear elastic materials, it finally yields a boundary integral relation for the stress at any interior point \mathbf{x} of the equivalent cracked half-space:

$$\sigma_{ik}(\mathbf{x}) = \int_{S_c^+} E_{ikpq} \frac{\partial \bar{U}_j^p(\xi, \mathbf{x})}{\partial x_q} \Sigma t_j(\xi) dA(\xi) - \int_{S_c^+} E_{ikpq} \frac{\partial \bar{S}_{ij}^p(\xi, \mathbf{x})}{\partial x_q} n_i^+(\xi) \Delta u_j(\xi) dA(\xi) \quad [4]$$

From the relations [1] and [2] along with the properties of the fundamental solutions $U_j^p(\xi - \mathbf{x})$ and $S_{ij}^p(\xi - \mathbf{x})$ for the uncracked whole space, the kernels $E_{ikpq} \partial \bar{U}_j^p(\xi, \mathbf{x}) / \partial x_q$ and $E_{ikpq} \partial \bar{S}_{ij}^p(\xi, \mathbf{x}) / \partial x_q$ contained in the boundary integral relation [4] can be further expressed as

$$E_{ikpq} \frac{\partial \bar{U}_j^p(\xi, \mathbf{x})}{\partial x_q} = -S_{ik}^j(\xi - \mathbf{x}) + \bar{\delta}_{jp} S_{ik}^p(\mathbf{x} - \bar{\xi}) \quad [5]$$

$$E_{ikpq} \frac{\partial \bar{S}_{ij}^p(\xi, \mathbf{x})}{\partial x_q} = -\Sigma_{ij}^{lk}(\xi - \mathbf{x}) - \bar{\delta}_{ia} \bar{\delta}_{jb} \Sigma_{ab}^{lk}(\mathbf{x} - \bar{\xi}) \quad [6]$$

where $\Sigma_{ij}^{lk}(\xi - \mathbf{x}) = E_{ikpq} \partial S_{ij}^p(\xi - \mathbf{x}) / \partial x_q$ and $\bar{\xi}$ is an image point of ξ with respect to the plane $x_3 = 0$. From the property of the stress fundamental solution for the uncracked whole space $S_{ij}^p(\xi - \mathbf{x})$, the kernels $E_{ikpq} \partial \bar{U}_j^p(\xi, \mathbf{x}) / \partial x_q$ and $E_{ikpq} \partial \bar{S}_{ij}^p(\xi, \mathbf{x}) / \partial x_q$ are clearly singular at $\xi = \mathbf{x}$ of $\mathcal{O}(1/r^2)$ and $\mathcal{O}(1/r^3)$, respectively. The two integral relations [3] and [4] form an essential basis for the development of governing integral equations for determining unknown crack-face data such as the sum of and the jump in the crack-face displacements. However, the direct use of those integral relations poses certain difficulties including the interpretation and numerical treatment of all involved strongly singular and hyper-singular integrals.

3.3 Regularized displacement and stress boundary integral relations

To regularize the boundary integral relations [3] and [4], special decompositions of involved strongly singular and hypersingular kernels are first established to aid the integration-by-part procedure. The essential component for establishing such decompositions is the special representations of the stress fundamental solution $S_{ij}^p(\xi - \mathbf{x})$ and the hypersingular kernel $\Sigma_{ij}^{lk}(\xi - \mathbf{x})$ for the uncracked whole space proposed by Rungamornrat and Mear (2008a). Such results are valid for generally anisotropic, linearly elastic materials and given explicitly by

$$S_{ij}^p(\xi - \mathbf{x}) = H_{ij}^p(\xi - \mathbf{x}) + \varepsilon_{ism} \frac{\partial}{\partial \xi_s} G_{mj}^p(\xi - \mathbf{x}) \quad [7]$$

$$\Sigma_{ij}^{lk}(\xi - \mathbf{x}) = -E_{ijkl} \delta(\xi - \mathbf{x}) + \varepsilon_{ism} \varepsilon_{lri} \frac{\partial}{\partial \xi_s} \frac{\partial}{\partial \xi_r} C_{mj}^{nk}(\xi - \mathbf{x}) \quad [8]$$

where ε_{ism} denotes an alternating symbol; $\delta(\xi - \mathbf{x})$ is a Dirac-delta distribution centered at \mathbf{x} ; and the functions $H_{ij}^p(\xi - \mathbf{x})$, $G_{mj}^p(\xi - \mathbf{x})$ and $C_{mj}^{nk}(\xi - \mathbf{x})$ are defined by

$$H_{ij}^p(\xi - \mathbf{x}) = -\delta_{ip} \frac{\xi_i - x_i}{4\pi r^3} \quad [9]$$

$$G_{mj}^p(\xi - \mathbf{x}) = \frac{\varepsilon_{mqsl} E_{qkl}}{8\pi^2 r} \oint_{z,r=0} (\mathbf{z}, \mathbf{z})_{kp}^{-1} z_q z_l ds(\mathbf{z}) \quad [10]$$

$$C_{mj}^{nk}(\xi - \mathbf{x}) = \frac{A_{misl}^{kijp}}{8\pi^2 r} \oint_{z,r=0} (\mathbf{z}, \mathbf{z})_{ap}^{-1} z_s z_l ds(\mathbf{z}) \quad [11]$$

where $A_{misl}^{kijp} = \varepsilon_{pid} \varepsilon_{pmq} (E_{dijp} E_{qkms} - E_{mpqs} E_{dijq} / 3)$; $\mathbf{r} = \xi - \mathbf{x}$; \mathbf{z} is a unit vector; (\mathbf{z}, \mathbf{z}) is a tensor whose components are defined by $(\mathbf{z}, \mathbf{z})_{kp} = z_m E_{mkpn} z_n$; and $(\mathbf{z}, \mathbf{z})^{-1}$ is the inverse of (\mathbf{z}, \mathbf{z}) . Note that the line integrals appearing in [10] and

[11] are traced along a unit circle $\|z\|=1$ on the plane $z \cdot r = 0$. It is evident from [9]-[11] that the functions $H_{ij}^p(\xi - x)$, $G_{mj}^p(\xi - x)$ and $C_{mj}^{rk}(\xi - x)$ are singular at $\xi = x$ of $\mathcal{O}(1/r^2)$, $\mathcal{O}(1/r)$ and $\mathcal{O}(1/r)$, respectively. By employing the relations [2] and [5] together with the decomposition [7], the stress fundamental solution $\bar{S}_{ij}^p(\xi, x)$ and the function $E_{lkpq} \partial \bar{U}_j^p(\xi, x) / \partial x_q$ for the uncracked half-space under the symmetric boundary conditions admits the representation

$$\bar{S}_{ij}^p(\xi, x) = \bar{H}_{ij}^p(\xi, x) + \varepsilon_{ism} \frac{\partial}{\partial \xi_s} \bar{G}_{mj}^p(\xi, x) \quad [12]$$

$$E_{lkpq} \frac{\partial \bar{U}_j^p(\xi, x)}{\partial x_q} = \bar{H}_{lk}^j(x, \xi) + \varepsilon_{lrt} \frac{\partial}{\partial x_r} \bar{G}_{lk}^j(x, \xi) \quad [13]$$

where the functions $\bar{H}_{ij}^p(\xi, x)$ and $\bar{G}_{mj}^p(\xi, x)$ are defined by

$$\bar{H}_{ij}^p(\xi, x) = H_{ij}^p(\xi - x) + \bar{\delta}_{pk} H_{ij}^k(\xi - \bar{x}) \quad [14]$$

$$\bar{G}_{mj}^p(\xi, x) = G_{mj}^p(\xi - x) + \bar{\delta}_{pk} G_{mj}^k(\xi - \bar{x}) \quad [15]$$

Finally, by applying the decomposition [8] to [6], it yields the representation of the kernel $E_{lkpq} \partial \bar{S}_{ij}^p(\xi, x) / \partial x_q$ as

$$E_{lkpq} \frac{\partial \bar{S}_{ij}^p(\xi, x)}{\partial x_q} = E_{ijld} \delta(\xi - x) - \bar{\delta}_{ia} \bar{\delta}_{jb} E_{abcd} \delta(x - \bar{\xi}) + \varepsilon_{ism} \varepsilon_{lrt} \frac{\partial}{\partial \xi_s} \frac{\partial}{\partial x_r} \bar{C}_{mj}^{rk}(\xi, x) \quad [16]$$

where the function $\bar{C}_{mj}^{rk}(\xi, x)$ is given by

$$\bar{C}_{mj}^{rk}(\xi, x) = C_{mj}^{rk}(\xi - x) - \bar{\delta}_{am} \bar{\delta}_{bj} C_{ab}^{rk}(x - \bar{\xi}) \quad [17]$$

From the singularity behavior of the functions $H_{ij}^p(\xi - x)$, $G_{mj}^p(\xi - x)$ and $C_{mj}^{rk}(\xi - x)$ indicated by [9]-[11], it is apparent from [14]-[15] and [17] that the functions $\bar{H}_{ij}^p(\xi, x)$, $\bar{G}_{mj}^p(\xi, x)$ and $\bar{C}_{mj}^{rk}(\xi, x)$ are singular only at a point $\xi = x$ of order $\mathcal{O}(1/r^2)$, $\mathcal{O}(1/r)$ and $\mathcal{O}(1/r)$, respectively.

By applying the decomposition [7] to the displacement boundary integral relation [3] and then integrating a term containing the function $\bar{G}_{mj}^p(\xi, x)$ by parts via Stokes' theorem, it finally results in

$$u_p(x) = \int_{S_c^+} \bar{U}_j^p(\xi, x) \Sigma_{t_j}(\xi) dA(\xi) - \int_{S_c^+} \bar{H}_{ij}^p(\xi, x) n_i^+(\xi) \Delta u_j(\xi) dA(\xi) + \int_{S_c^+} \bar{G}_{mj}^p(\xi, x) D_m \Delta u_j(\xi) dA(\xi) \quad [18]$$

where $D_m(\cdot) = n_i \varepsilon_{ism} \partial(\cdot) / \partial \xi_s$ denotes a surface differential operator. The boundary term resulting from the integration by part vanishes due to the enforcement of the closure condition along the crack front (i.e., $\Delta u_j(\xi) = 0 \forall \xi \in \partial S_c^+$). It is worth noting that the boundary

integral relation [18] contains only weakly singular kernels of $\mathcal{O}(1/r)$. The weak singularity of the product $\bar{H}_{ij}^p(\xi, x) n_i^+(\xi)$ results directly from the relation [14] and the property of the function $H_{ij}^p(\xi - x)$, as pointed out before by Xiao (1998). Similarly, by applying the decompositions [13] and [16] to the boundary integral relation for the stress [4] and then integrating the term associated with the kernel $\bar{C}_{mj}^{rk}(\xi, x)$ by parts via Stokes' theorem, it finally leads to

$$\sigma_{ik}(x) = \varepsilon_{lrt} \frac{\partial}{\partial x_r} \left\{ \int_{S_c^+} \bar{C}_{mj}^{rk}(\xi, x) D_m \Delta u_j(\xi) dA(\xi) + \int_{S_c^+} \bar{G}_{lk}^j(x, \xi) \Sigma_{t_j}(\xi) dA(\xi) \right\} + \int_{S_c^+} \bar{H}_{lk}^j(x, \xi) \Sigma_{t_j}(\xi) dA(\xi) \quad [19]$$

where the closure condition has been enforced again and the contribution of the Dirac-delta distributions disappear at any interior point x . A pair of singularity-reduced boundary integral relations [18] and [19] forms the basis for the post-process of the displacement and stress at any interior point x once the unknown jump in the crack-face displacement (i.e., Δu_j) is fully determined.

3.4 Weakly singular, weak-form integral equations for equivalent cracked half-space

By properly forming the limit $x \rightarrow y \in S_c^+$ of the regularized boundary integral relation [18], it yields the boundary integral equation for the sum of the crack-face displacement as

$$c(y) \Sigma u_p(y) = \int_{S_c^+} \bar{U}_j^p(\xi, y) \Sigma_{t_j}(\xi) dA(\xi) + \int_{S_c^+} \bar{G}_{mj}^p(\xi, y) D_m \Delta u_j(\xi) dA(\xi) - \int_{S_c^+} \bar{H}_{ij}^p(\xi, y) n_i^+(\xi) \Delta u_j(\xi) dA(\xi) \quad [20]$$

where $\Sigma u_p(y) = u_p(y^+) + u_p(y^-)$ denotes the sum of the crack-face displacement and the function $c = c(y)$ is defined such that $0 < c(y) < 1$ and $c(y) = 1/2$ if the surface is sufficiently smooth at y . By multiplying [20] by a sufficiently smooth test function $\tilde{t}_p(y)$ and then integrating the result over S_c^+ , it leads to a weakly-singular, weak-form boundary integral equation for the sum of the crack-face displacement:

$$\frac{1}{2} \int_{S_c^+} \tilde{t}_p(y) \Sigma u_p(y) dA(y) = \int_{S_c^+} \tilde{t}_p(y) \int_{S_c^+} \bar{U}_j^p(\xi, y) \Sigma_{t_j}(\xi) dA(\xi) dA(y) + \int_{S_c^+} \tilde{t}_p(y) \int_{S_c^+} \bar{G}_{mj}^p(\xi, y) D_m \Delta u_j(\xi) dA(\xi) dA(y) - \int_{S_c^+} \tilde{t}_p(y) \int_{S_c^+} \bar{H}_{ij}^p(\xi, y) n_i^+(\xi) \Delta u_j(\xi) dA(\xi) dA(y) \quad [21]$$

It is important to emphasize that the function $c = c(y)$ simply reduces to 1/2 since the crack surface is assumed

piecewise smooth (i.e., a set of points y whose unit normal vector is not well-defined is of measure zero). Clearly, the weak-form boundary integral equation [21] contains only weakly singular kernels of $\mathcal{O}(1/r)$.

To establish the weakly singular, weak-form boundary integral equation for the crack-face traction, we first form the product $n_i^+(y)\sigma_{ik}(x)$, $y \in S_c^+$ using the boundary integral relation [19] and then take the limit $x \rightarrow y$. This process yields the following singularity-reduced boundary integral equation for the crack-face traction

$$\rho(y)\Delta t_k(y) = D_t \left\{ \int_{S_c^+} \bar{C}_{mj}^{ik}(\xi, y) D_m \Delta u_j(\xi) dA(\xi) + \int_{S_c^+} \bar{G}_{ik}^j(y, \xi) \Sigma t_j(\xi) dA(\xi) \right\} + n_i^+(y) \int_{S_c^+} \bar{H}_{ik}^j(y, \xi) \Sigma t_j(\xi) dA(\xi) \quad [22]$$

where $\Delta t_k(y) = t_k(y^+) - t_k(y^-)$ denotes the jump in the crack-face traction and $\rho = \rho(y)$ is defined such that $0 < \rho(y) < 1$ and $\rho(y) = 1/2$ if the surface is sufficiently smooth at y . By multiplying the boundary integral equation [22] by a sufficiently smooth test function $\tilde{u}_k(y)$, integrating the result over the crack surface S_c^+ , then performing an integration by parts via Stokes' theorem of integrals containing the kernels $\bar{C}_{mj}^{ik}(\xi, x)$ and $\bar{G}_{ik}^j(y, \xi)$, and finally choosing the test function $\tilde{u}_k(y)$ to satisfy the closure condition along the crack front (i.e., $\tilde{u}_k(y) = 0 \forall y \in \partial S_c^+$), it gives rise to

$$\begin{aligned} \frac{1}{2} \int_{S_c^+} \tilde{u}_k(y) \Delta t_k(y) dA(y) &= \int_{S_c^+} \tilde{u}_k(y) \int_{S_c^+} \bar{H}_{ik}^j(y, \xi) n_i^+(y) \Sigma t_j(\xi) dA(\xi) dA(y) \\ &\quad - \int_{S_c^+} D_i \tilde{u}_k(y) \int_{S_c^+} \bar{G}_{ik}^j(y, \xi) \Sigma t_j(\xi) dA(\xi) dA(y) \\ &\quad - \int_{S_c^+} D_i \tilde{u}_k(y) \int_{S_c^+} \bar{C}_{mj}^{ik}(\xi, y) D_m \Delta u_j(\xi) dA(\xi) dA(y) \end{aligned} \quad [23]$$

Again, from the piecewise smoothness of the crack surface, the function $\rho = \rho(y)$ simply reduces to 1/2. It is also important to point out that the weak-form, traction boundary integral equation [23] contains only weakly singular kernels of $\mathcal{O}(1/r)$.

4. Solution methodology

A pair of weakly singular, weak-form boundary integral equations [21] and [23] provides the essential basis for the formulation of the boundary value problem of the equivalent cracked half-space shown in **Fig. 1(b)**. The final governing equations contain only unknowns on the crack surface including the sum of the crack-face displacement Σu_p and the jump in the crack-face displacement Δu_p . It is apparent that the weakly-singular, weak-form traction boundary integral equation [23] contains the complete information of the prescribed crack-face tractions (i.e., Δt_i and Σt_i) and is independent

of the unknown Σu_p . The solution of the jump in the crack-face displacement Δu_p can be, therefore, determined by solving this weak-form equation. Once the data Δu_p is fully obtained, it is then employed together with the weak-form integral equation [21] to solve for the unknown sum of the crack-face displacement Σu_p .

In the present study, a symmetric Galerkin boundary element method (SGBEM) is adopted to construct the numerical solution of the weak-form equation [23] (also see the work of Rungamornrat and Mear (2008b), Li et al. (1998), Frangi et al. (2002)). Due to the weakly singular nature of all involved integrals, continuous finite element basis functions are employed everywhere in the approximation; in particular, 6-node, 8-node, and 9-node quadratic elements are employed in the discretization of the crack surface. To further enhance the accuracy of the approximation, special 9-node crack-tip elements proposed by Rungamornrat and Mear (2008b) and Li et al. (1998) are adopted to discretize the jump in the crack-face displacement in a region adjacent to the crack front. Such special crack-tip elements possess two positive features including their shape functions properly enriched by a square-root function and extra degrees of freedom introduced along the crack front to represent the gradient of the jump in the crack-face displacement. The former feature allows the near-front solution to be captured accurately using relatively coarse meshes whereas the latter renders the stress intensity factors to be extracted directly from those extra degrees of freedom without carrying the extrapolation. To form a system of linear algebraic equations resulting from the discretization, two essential tasks are accomplished with a special care. One is associated with the numerical evaluation of regular, weakly singular and nearly singular integrals over elements or pairs of elements resulting from the discretization procedure. The regular integrals including both single surface and double surface integrals over pairs of remote elements are integrated efficiently and accurately by standard Gaussian quadrature. For the last two types of integrals, the weak singularity and rapid variation of integrands induced when pairs of coincident or adjacent elements are involved renders the integrals very difficult to be evaluated by standard Gaussian quadrature (e.g., Xiao, 1998). In the present study, an integrand-regularization technique similar to that proposed by Xiao (1998) is employed to efficiently integrate those double surface integrals. Specifically, a family of variable transformations such as triangular-polar transformation and logarithmic transformations is applied to either remove the weak singularity or alleviate the fast variation of the integrand before they are integrated by standard Gaussian quadrature. The other important task corresponds directly to the evaluation of all involved

kernels $\bar{H}_{ij}^p(\xi, x)$, $\bar{G}_{mj}^p(\xi, x)$ and $\bar{C}_{mj}^{nk}(\xi, x)$ for every pair of points (ξ, x) resulting from the numerical quadrature. It is evident from the relations [14], [15] and [17] that such task only requires calculations of the kernels $H_{ij}^p(\xi - x)$, $G_{mj}^p(\xi - x)$ and $C_{mj}^{nk}(\xi - x)$ for the uncracked whole space. Since $H_{ij}^p(\xi - x)$, is independent of material property and involves only elementary functions, its evaluation can be readily achieved via the direct substitution. On the contrary, the kernels $G_{mj}^p(\xi - x)$ and $C_{mj}^{nk}(\xi - x)$ are material dependent and the direct evaluation by performing all involved contour integrals for every pair of points (ξ, x) is computationally expensive. To avoid such massive calculations, an interpolation scheme similar to that used by Rungamornrat and Mear (2008b) is adopted. In this technique, the kernels $G_{mj}^p(\xi - x)$ and $C_{mj}^{nk}(\xi - x)$ given by [10] and [11] are first rewritten as a product of two parts:

$$G_{mj}^p(\xi - x) = \frac{\varepsilon_{mqa} E_{qkl}}{8\pi^2 r} \times I_{ij}^{ql}(\theta, \phi) \tag{24}$$

$$C_{mj}^{nk}(\xi - x) = \frac{A_{msl}^{kjp}}{8\pi^2 r} \times I_{ap}^{sl}(\theta, \phi) \tag{25}$$

where $r = \|\xi - x\|$, $\theta \in [0, 2\pi]$, $\phi \in [0, \pi]$ denote spherical coordinates of point ξ with the origin at point x and the angular dependent function $I_{ij}^{kl}(\theta, \phi)$ is defined by

$$I_{ij}^{kl}(\theta, \phi) = \oint_{z=r=0} (z, z)_{ij}^{-1} z_k z_l ds(z) \tag{26}$$

It is evident that the first part of both kernels involves mainly elementary functions and can, therefore, be calculated efficiently via the direct substitution. For the second part, the function $I_{ij}^{kl}(\theta, \phi)$ is approximated over a domain $[0, 2\pi] \times [0, \pi]$ using finite element interpolations. In such procedure, the direct evaluation of the line integral [26] is only required at nodal points and it can be achieved efficiently via Gaussian quadrature. The accuracy of the approximation can be readily controlled and enhanced by refining the interpolation grid. The final, symmetric, dense system of linear algebraic equations is then solved by a selected efficient indirect linear solver such as a preconditioning conjugate gradient method.

To determine the sum of the crack-face displacement Σu_p , the weak-form boundary integral equation [21] is subsequently solved by a standard Galerkin technique. Note that once the jump in the crack-face displacement Δu_p is obtained, all double surface integrals appearing on the right hand side of [21] serve only as the prescribed data and the single surface integral containing the unknown Σu_p is relatively simple. Due to the regularity behavior of Σu_p over the entire crack surface, standard two-dimensional isoparametric elements are adopted everywhere in the discretization of trial and test functions. Essential ingredients described above also apply to treat

all involved single surface and double surface integrals and the calculations of all kernels. The resulting, symmetric, sparse system of linear algebraic equations is then efficiently solved by the same indirect linear solver.

5. Post-process

Once the unknown crack-face data $\{\Sigma u_p, \Delta u_p\}$ are obtained, other related quantities such as the displacements and stresses at any point within the cracked medium and the stress intensity factors and T-stress components along the crack front can be determined. The former can be readily computed using the singularity-reduced boundary integral relations [18] and [19] whereas the post-process of the latter from the local stress field in the neighborhood of the crack front still requires non-trivial treatment of nearly singular integrals and limiting procedure. To avoid difficulties posed in such task, the solved crack-face displacement data (i.e., Σu_p and Δu_p) is utilized, instead, to extract the stress intensity factors and the T-stress components. Such procedure is briefly summarized as follows (see also the work of Rungamornrat and Mear (2008b), Li et al. (1998), Pham (2015) and Rungamornrat et al. (2018)).

Let x_c be a point on the crack front and $\{x_c; \bar{x}_1, \bar{x}_2, \bar{x}_3\}$ be a local Cartesian coordinate system with the origin at x_c and the orthonormal base vectors $\{\bar{e}_1, \bar{e}_2, \bar{e}_3\}$. In particular, $\{\bar{e}_1, \bar{e}_2, \bar{e}_3\}$ are chosen such that \bar{e}_3 is tangent to the crack front at x_c ; \bar{e}_2 is normal to the crack surface S_c^+ at x_c and $\bar{e}_2 = -n^+$; and $\bar{e}_1 = \bar{e}_2 \times \bar{e}_3$ is normal to the crack front and directs inside the medium as clearly indicated in Fig. 3. By using the property of special crack-tip elements, Li et al. (1998) and Rungamornrat and Mear (2008b) proposed an explicit formula for determining the mixed-mode stress intensity factors (K_I, K_{II}, K_{III}) in terms of the extra nodal degrees of freedom placed along the crack front as

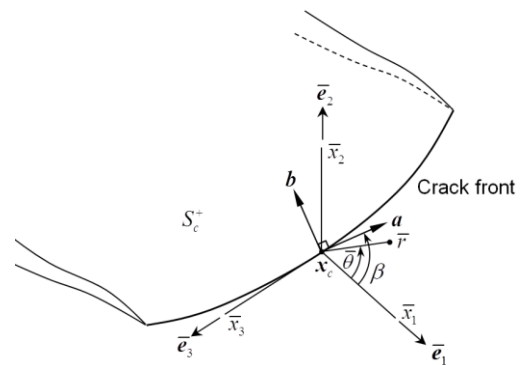


Fig. 3. Local Cartesian coordinate system and all involved parameters for determining stress intensity factors and T-stress components.

$$k_i(x_c) = \sqrt{\frac{\pi}{2\gamma}} B_{ij} [\hat{u}(x_c) \cdot \bar{e}_j] \quad [27]$$

where $k_1 \equiv K_{II}$, $k_2 \equiv K_I$, $k_3 \equiv K_{III}$;

$$\gamma = -\bar{e}_1 \cdot \frac{\partial \mathbf{r}_c}{\partial \eta}(\xi_c, -1), \quad [28]$$

$$\mathbf{r}_c = \sum_{i=1}^9 \mathbf{x}^{(i)} \psi^{(i)}(\xi, \eta) - \mathbf{x}_c, \quad [29]$$

$$\hat{u}(x_c) = \sum_i \Delta u^{(i)} \psi^{(i)}(\xi_c, -1); \quad [30]$$

$\mathbf{x}^{(i)}$ is the i^{th} node of the crack-tip element; $(\xi, \eta) \in [-1, 1] \times [-1, 1]$ are master coordinates of any point within the crack-tip element and $(\xi_c, -1)$ are master coordinates of the point x_c ; $\psi^{(i)}(\xi, \eta)$ is a standard quadratic shape function of the i^{th} node defined on a 9-node master element; $\Delta u^{(i)}$ represents the extra degree of freedom of the i^{th} node of the crack-tip element along the crack front; and B_{ij} is given by

$$B_{ij} = \frac{1}{2\pi} \int_0^{2\pi} [(a, a)_{ij} - (a, b)_{im} (b, b)_{mn}^{-1} (b, a)_{nj}] d\beta \quad [31]$$

with a and b denoting orthonormal vectors in the plane $\bar{x}_3 = 0$ and β denoting the angle between a and the unit vector \bar{e}_1 as indicated in **Fig. 3**. It is worth noting that the summation in [30] is taken only over nodes of the crack-tip element located along the crack front.

The T-stress components along the boundary of the crack can be also obtained directly from the sum of the crack-face displacement as described below. First, the finite part of the stress tensor at the point x_c along the crack front, with $T_{ij}(x_c)$ denoting its local components, is related to the finite part of the strain tensor at the same point, with $\bar{\varepsilon}_{kl}(x_c)$ denoting its local components, by

$$T_{ij}(x_c) = \bar{E}_{ijkl}(x_c) \bar{\varepsilon}_{kl}(x_c) \quad [32]$$

where $\bar{E}_{ijkl}(x_c)$ are local components of the elastic moduli at x_c . From the continuity of the finite part of the stress at x_c , three local components T_{12} , T_{22} , and T_{23} are, therefore, known a priori and can be obtained from the prescribed crack-face traction at x_c . In addition, three in-plane components of $\bar{\varepsilon}_{kl}(x_c)$ at x_c can be computed from the solved sum of the crack-face displacement as

$$\begin{aligned} \bar{\varepsilon}_{11}(x_c) &= \frac{1}{2} \frac{\partial \Sigma \bar{u}_1(x_c)}{\partial \bar{x}_1}; \bar{\varepsilon}_{33}(x_c) = \frac{1}{2} \frac{\partial \Sigma \bar{u}_3(x_c)}{\partial \bar{x}_3}; \\ \bar{\varepsilon}_{13}(x_c) &= \frac{1}{4} \frac{\partial \Sigma \bar{u}_1(x_c)}{\partial \bar{x}_3} + \frac{1}{4} \frac{\partial \Sigma \bar{u}_3(x_c)}{\partial \bar{x}_1} \end{aligned} \quad [33]$$

The derivatives involved in the expressions [33] can be carried out directly within elements along the crack front. From the prescribed information of T_{12} , T_{22} , and T_{23} and

the computed components $\bar{\varepsilon}_{11}$, $\bar{\varepsilon}_{13}$ and $\bar{\varepsilon}_{33}$, the unknown components T_{11} , T_{13} , and T_{33} at any point x_c along the crack front, commonly termed the T-stress components, can be obtained by solving a system of six independent linear algebraic equations [32].

6. Numerical results

In this section, the boundary integral formulation and the implemented solution procedure for a cracked whole space possessing a plane of symmetry is fully tested. Three different boundary value problems are considered to demonstrate the computational performance and robustness of the proposed technique. In numerical simulations, two representative, linearly elastic materials, one for isotropic and the other for transversely isotropic solids, with elastic constants shown in **Table 1** are employed. For the transversely isotropic material, the axis of material symmetry is taken to direct normal to the plane of symmetry, i.e., the $x_1 - x_2$ plane. Special 9-node crack-tip elements are used to discretize the region adjacent to the crack front whereas standard 8-node quadrilateral elements and 6-node triangular elements are adopted to discretize the majority of the crack surface.

6.1 Pair of identical horizontal penny-shaped cracks

Consider, first, a pair of identical horizontal penny-shaped cracks embedded in a whole space and the distance from their surfaces to the symmetric plane is h as shown in **Fig. 4(a)**. The crack radius is denoted by a and the lower crack front is parameterized by $x_1 = a \cos \beta$, $x_2 = -a \sin \beta$, $x_3 = h$ for $\beta \in [0, 2\pi]$. The equivalent cracked half-space under the symmetric boundary conditions is indicated in **Fig. 4(b)** and each crack is subjected to a uniform traction $t_1^+ = -t_1^- = -\sigma_0$, $t_2^+ = -t_2^- = 0$, $t_3^+ = -t_3^- = -\sigma_0$, (see **Fig. 4(c)**). In the analysis, four meshes are adopted as indicated in **Fig. 4(d)** and the normalized depth $h/a = 0.5$ is considered.

Computed stress intensity factors and T-stress components at $\beta = 0^\circ, 90^\circ$ and 180° are normalized by the

Table 1. Elastic constants for isotropic material (associated with Poisson's ratio $\nu = 0.3$ and $E = 2.6$ GPa) and transversely isotropic material with the axis of material symmetry normal to half-space surface.

| Materials | Elastic constants (GPa) | | | | |
|------------------------|-------------------------|------------|------------|------------|------------|
| | E_{1111} | E_{1122} | E_{1133} | E_{2222} | E_{1313} |
| Isotropic | 3.500 | 1.500 | 1.500 | 3.500 | 1.000 |
| Transversely isotropic | 16.090 | 3.350 | 5.010 | 6.100 | 3.830 |

reference solution and then reported in **Tables 2** and **3**. It is remarked that the reference results are taken as the solution of a cracked whole space shown in **Fig. 4(a)**

without exploiting the symmetry by the SGBEM proposed by Rungamornrat and Mear (2008b) with use of the Mesh 4. As can be seen from results in **Table 2**, numerical

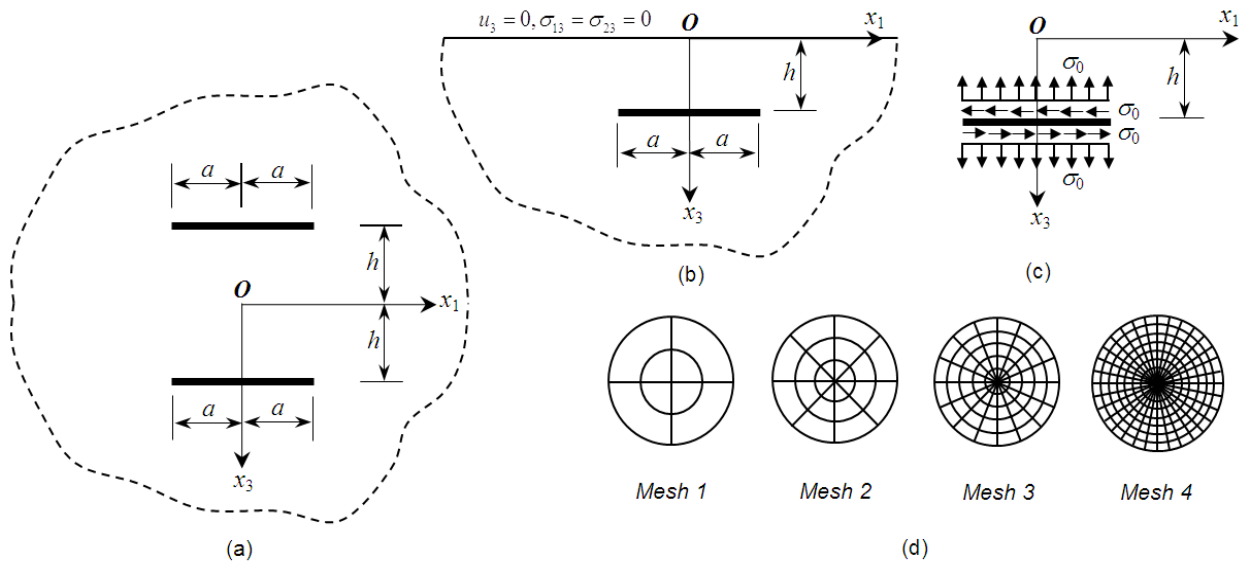


Fig. 4. Schematics of (a) pair of identical, horizontal penny-shaped cracks in whole space, (b) equivalent cracked half-space, (c) tractions acting on crack surfaces, and (d) four meshes used in analysis.

Table 2. Normalized stress intensity factors at $\beta = 0^\circ, 90^\circ$ and 180° for lower penny-shaped crack shown in **Fig. 4(a)** with $h/a = 0.5$.

| β | Mesh | Isotropic | | | Transversely isotropic | | |
|-------------|------|-------------------|-------------------------|---------------------------|------------------------|-------------------------|---------------------------|
| | | K_I / K_I^{ref} | K_{II} / K_{II}^{ref} | K_{III} / K_{III}^{ref} | K_I / K_I^{ref} | K_{II} / K_{II}^{ref} | K_{III} / K_{III}^{ref} |
| 0° | 1 | 0.9949 | 0.9896 | - | 0.9928 | 0.9907 | - |
| | 2 | 1.0004 | 1.0001 | - | 1.0000 | 1.0004 | - |
| | 3 | 1.0003 | 1.0002 | - | 1.0002 | 1.0004 | - |
| 90° | 1 | 0.9935 | 1.0011 | 0.9817 | 0.9927 | 0.9903 | 0.9835 |
| | 2 | 1.0002 | 1.0016 | 0.9990 | 1.0000 | 1.0000 | 0.9994 |
| | 3 | 1.0003 | 1.0004 | 1.0000 | 1.0002 | 1.0000 | 1.0002 |
| 180° | 1 | 0.9916 | 0.9911 | - | 0.9927 | 0.9907 | - |
| | 2 | 1.0000 | 1.0003 | - | 1.0000 | 1.0003 | - |
| | 3 | 1.0002 | 1.0002 | - | 1.0002 | 1.0003 | - |

Table 3. Normalized T-stress components at $\beta = 0^\circ, 90^\circ$ and 180° for lower penny-shaped crack shown in **Fig. 4(a)** with $h/a = 0.5$.

| β | Mesh | Isotropic | | | Transversely isotropic | | |
|-------------|------|-------------------------|---------------------------|---------------------------|-------------------------|---------------------------|---------------------------|
| | | T_{11} / T_{11}^{ref} | T_{33}^* / T_{33}^{ref} | T_{13}^* / T_{13}^{ref} | T_{11} / T_{11}^{ref} | T_{33}^* / T_{33}^{ref} | T_{13}^* / T_{13}^{ref} |
| 0° | 1 | 1.0359 | 1.0252 | - | 1.0184 | 1.0055 | - |
| | 2 | 1.0186 | 1.0166 | - | 1.0075 | 1.0057 | - |
| | 3 | 1.0055 | 1.0049 | - | 1.0023 | 1.0017 | - |
| 90° | 1 | 1.0037 | 0.9988 | 0.9626 | 1.0063 | 0.9969 | 1.0787 |
| | 2 | 1.0042 | 1.0013 | 1.1549 | 1.0034 | 0.9995 | 1.0825 |
| | 3 | 1.0021 | 1.0008 | 1.0662 | 1.0015 | 0.9999 | 1.0297 |
| 180° | 1 | 0.9658 | 0.9603 | - | 0.9930 | 0.9868 | - |
| | 2 | 0.9873 | 0.9790 | - | 0.9989 | 0.9921 | - |
| | 3 | 0.9980 | 0.9947 | - | 1.0006 | 0.9977 | - |

solutions exhibit excellent agreement with the reference solutions for the first three meshes and they are weakly dependent on the level of mesh refinement. In particular, the discrepancy between the stress intensity factors generated by the coarsest and intermediate meshes and the reference solutions is less than 1.9% and 0.2% for the isotropic case and 1.7% and 0.1% for the transversely isotropic case, respectively, whereas results obtained from the Mesh 3 are nearly identical to the reference solution. The high quality of the numerical solutions, while employing relatively coarse meshes, is the direct consequence of the use of special crack-tip elements to enhance the near-front approximation of the relative crack-face displacement.

Similar convergence behavior can be also observed for results of the T-stress components shown in **Table 3**; however, it is apparent that the difference between the computed solutions T_{13} from the Mesh 1 and Mesh 2 and the reference solution is larger than the case of the stress intensity factors. The reduction in the accuracy results directly from the fact that the derivatives of the sum of the crack-face displacement are required in the calculation of the T-stress components.

6.2 Pair of identical vertical penny-shaped cracks

Consider, next, a pair of identical, vertical penny-shaped cracks of radius a embedded in a whole space with a depth h (measured from the center of each crack to the plane of symmetry) as illustrated in **Fig. 5(a)**. The lower crack front is parameterized by $x_1 = 0$, $x_2 = a \sin \beta$, $x_3 = h - a \cos \beta$ for $\beta \in [0, 2\pi]$. The equivalent cracked half-space subjected to symmetric boundary conditions is

shown in **Fig. 5(b)** and each crack is subjected to the uniformly distributed, self-equilibrated, normal tractions $t_1^+ = -t_1^- = -\sigma_0$, $t_2^+ = -t_2^- = 0$, $t_3^+ = -t_3^- = 0$ (see **Fig. 5(c)**). It is apparent from the symmetry of the crack-face loading about the plane $x_1 = 0$ that the mode-II and mode-III stress intensity factors identically vanish along the crack front. In the numerical study, four meshes of the penny-shaped crack are adopted as illustrated in **Fig. 5(d)** and the aspect ratio with $h/a = 1.25$ is considered.

The computed mode-I stress intensity factor and T-stress components for both isotropic and transversely isotropic materials are normalized by the reference solution (taken from the converged SGBEM solution of a cracked whole space shown in **Fig. 5(a)** without exploiting the symmetry) and then reported in **Figs. 6** and **7**. As can be seen from results in **Fig. 6**, the computed mode-I stress intensity factor shows very good agreement with the reference solution for all three meshes and both types of materials. Similarly, numerical solutions for the T-stress components shown in **Fig. 7** for both materials also indicate the good convergence behavior and the weak dependence on the level of mesh refinement. Evidently, results generated by the coarsest mesh, intermediate mesh and finest mesh are nearly indistinguishable from the benchmark solution. The high quality of the numerical solutions results directly, again, from the use of special crack-tip elements to capture the near-front relative crack-face displacement.

6.3 Vertical penny-shaped crack under non-uniform tractions

Consider, as a final example, a circular crack of radius a

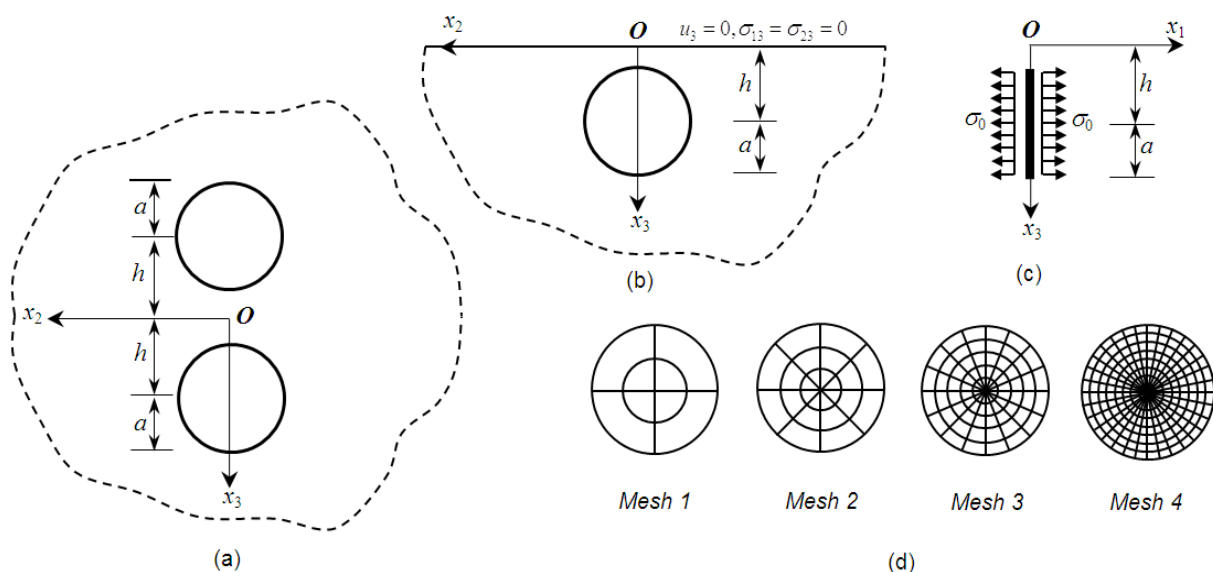


Fig. 5. Schematics of (a) pair of identical, vertical penny-shaped cracks in whole space, (b) equivalent cracked half-space, (c) tractions acting on crack surfaces, and (d) four meshes used in analysis.

embedded in a whole space and oriented perpendicular to the plane of symmetry, i.e., the plane $x_3 = 0$, as shown schematically in **Fig. 8(a)**. The equivalent cracked half-space under the symmetric boundary conditions used in the analysis is also illustrated in **Fig. 8(b)**. The corresponding semi-circular crack front is parameterized by $x_1 = -a \cos \beta$, $x_2 = 0$, $x_3 = a \sin \beta$ for $\beta \in [0, 2\pi]$. To demonstrate the capability of the proposed technique to treat general loading conditions, three types of symmetric, self-equilibrated, crack-face tractions including the non-uniform normal traction $t_1^+ = t_3^+ = 0, t_2^+ = -\sigma_0(x_3/a)^2$, the non-uniform horizontal shear traction $t_2^+ = t_3^+ = 0, t_1^+ = \sigma_0(x_3/a)^2$, and the non-uniform vertical shear traction $t_1^+ = t_2^+ = 0,$

$t_3^+ = \sigma_0(x_3/a)^2$ are treated (as indicated in **Fig. 9**). Three meshes as indicated in **Fig. 8(c)** are adopted in the analysis and the reference solution associated with the cracked whole-space shown in **Fig. 8(a)** without using the symmetry is obtained via the weakly singular SGBEM (Rungamornrat and Mear, 2008b).

For the first loading condition (see **Fig. 9(a)**), the mode-II and mode-III stress intensity factors vanish whereas the mode-I stress intensity factor and all T-stress components vary along the crack front. The computed mode-I stress intensity factor and T-stress components are reported in **Figs. 10** and **11**, respectively, for both isotropic and transversely isotropic materials. In

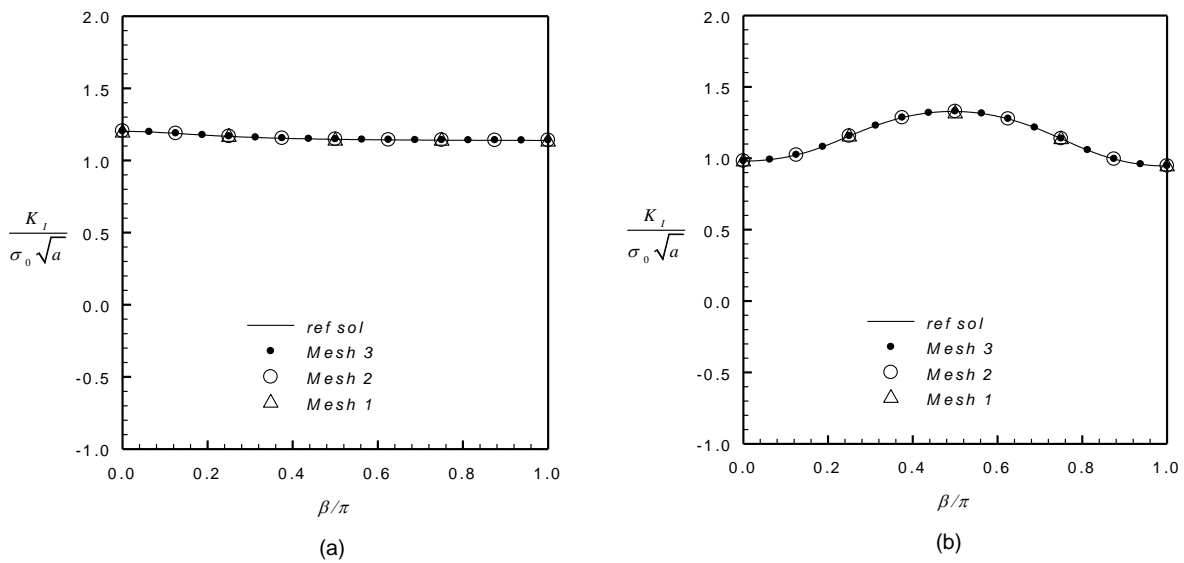


Fig. 6. Normalized mode-I stress intensity factors of lower penny-shaped crack under uniform normal traction for (a) isotropic case and (b) transversely isotropic case.

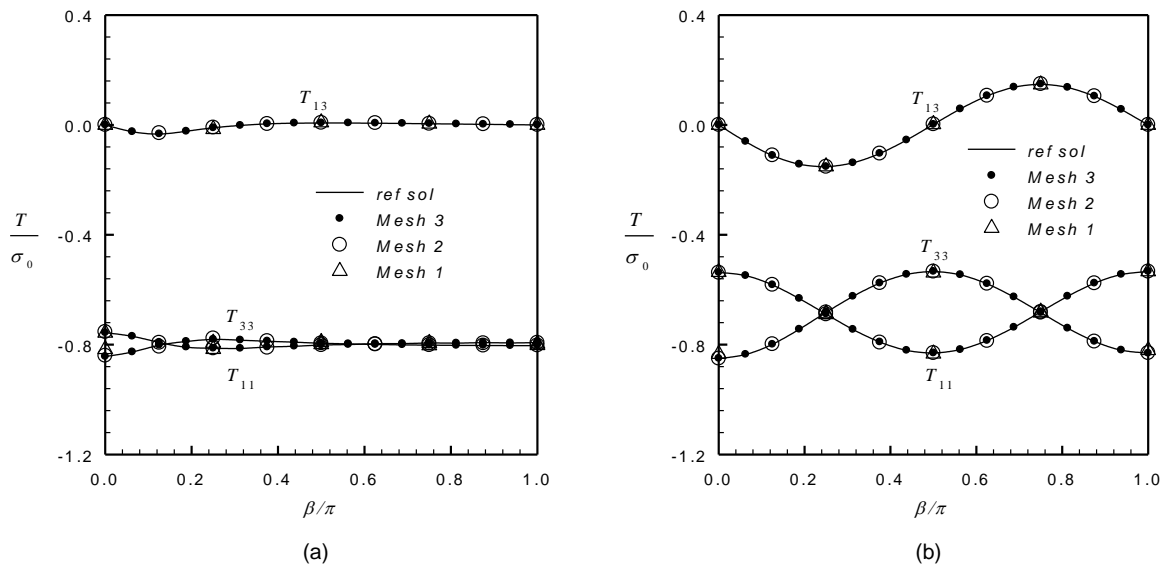


Fig. 7. Normalized T-stress components of lower penny-shaped crack under uniform normal traction for (a) isotropic case and (b) transversely isotropic case.

addition to the good agreement between the computed results and the reference solution and the weak dependence on the level of discretization, it can be also seen that the influence of the material anisotropy on the value and distribution of the mode-I stress intensity factor and all T-stress components along the crack front is not significant. For the second and third loading conditions, the applied shear traction in either x_1 – direction or x_3 – direction yields zero mode-I stress intensity factor and all zero T-stress components along the entire crack front. Computed mode-II and mode-III stress intensity factors of such shear loading conditions are reported in **Figs. 12** and **13** for all three meshes and both materials together with the reference solution. Similar to the previous case, this set of results indicates that the proposed technique with use of special crack-tip elements yields highly accurate stress intensity factors comparable to the reference solution for all meshes employed. In addition, use of the symmetry or the equivalent cracked half-space in the analysis can

significantly reduce the number of degrees of freedom in comparison with the treatment of the whole cracked space. In particular, a semi-circular crack is discretized instead of the entire penny-shaped crack.

7. Conclusions and remarks

A set of singularity-reduced integral representations has been established for the analysis of cracks in an anisotropic, linearly elastic, whole space possessing a plane of symmetry. The systematic regularization procedure based on the derivative transferring technique via the integration by parts and Stokes’ theorem has been utilized along with special decompositions of strongly singular and hypersingular kernels to derive a pair of weakly singular, weak-form boundary integral equations governing the unknown crack-face data for the equivalent cracked half-spaces. Another key feature of the developed integral equations, in addition to the

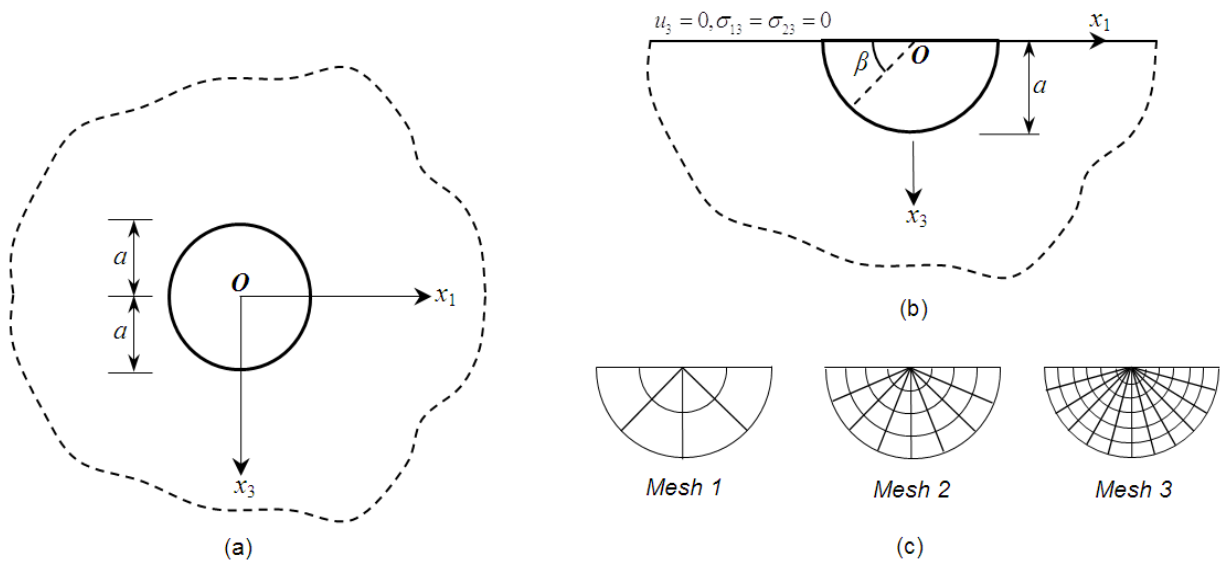


Fig. 8. Schematics of (a) vertical penny-shaped crack in elastic whole space, (b) equivalent cracked half-space, and (c) three meshes used in analysis.

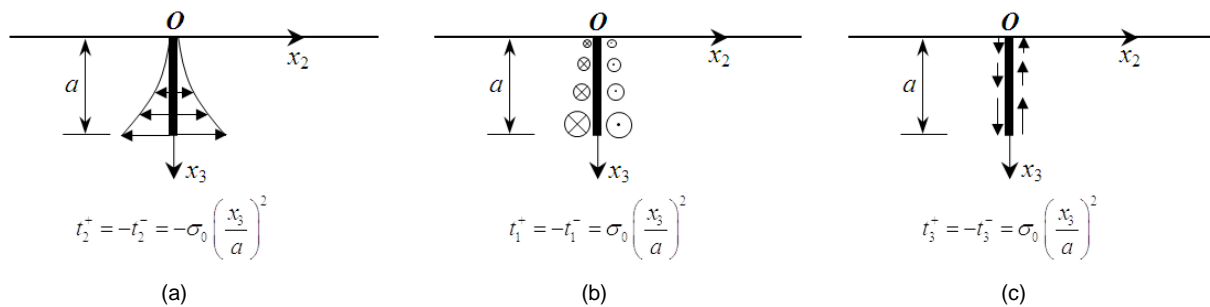


Fig. 9. Schematics of crack under (a) non-uniform normal traction $t_2^+ = t_2^- = -\sigma_0(x_3/a)^2$, (b) non-uniform horizontal shear traction $t_1^+ = t_1^- = \sigma_0(x_3/a)^2$, and (c) non-uniform vertical shear traction $t_3^+ = t_3^- = \sigma_0(x_3/a)^2$.

weakly singular nature, is the automatic treatment of the existing symmetry via the use of fundamental solutions of the half-space under symmetric boundary conditions on the free surface. This therefore avoids the discretization of the free surface in the solution procedure.

The weakly singular symmetric Galerkin boundary element method (SGBEM) and standard Galerkin finite element technique have been successfully implemented to solve a pair of weakly-singular, weak-form traction boundary integral equations for the sum of and the jump in the crack-face displacement. Special crack-tip elements have been also employed in the solution discretization to enhance the approximation of the near-

front relative crack-face displacement. Essential fracture data along the crack front such as the stress intensity factors and the T-stress components has been directly post-processed from the solved data of the crack-face displacements using the explicit formula. Results from extensive numerical experiments and the comparison with several benchmarked cases have revealed that the proposed numerical procedure is highly accurate and computationally robust for the analysis of a cracked half-space under the symmetric boundary conditions. Use of the special crack-tip elements along the crack front has indicated that the stress intensity factors can be accurately captured using relatively very coarse meshes

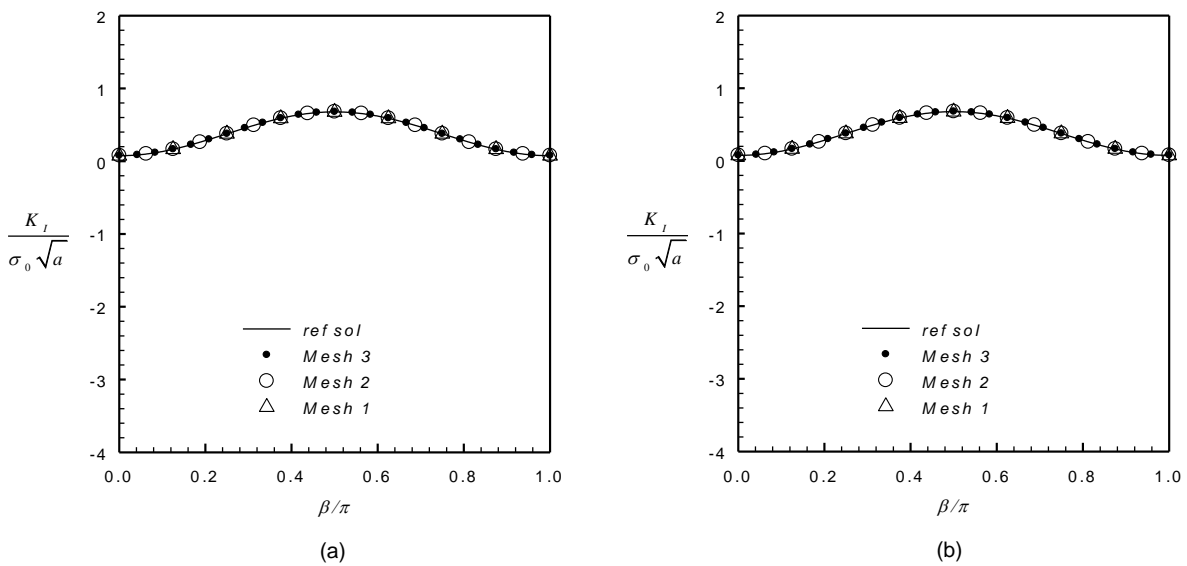


Fig. 10. Normalized mode-I stress intensity factor for vertical crack in whole space subjected to self-equilibrated, non-uniform normal traction $t_1^+ = t_3^+ = 0, t_2^+ = -\sigma_0(x_3/a)^2$ for (a) isotropic material and (b) transversely isotropic material.

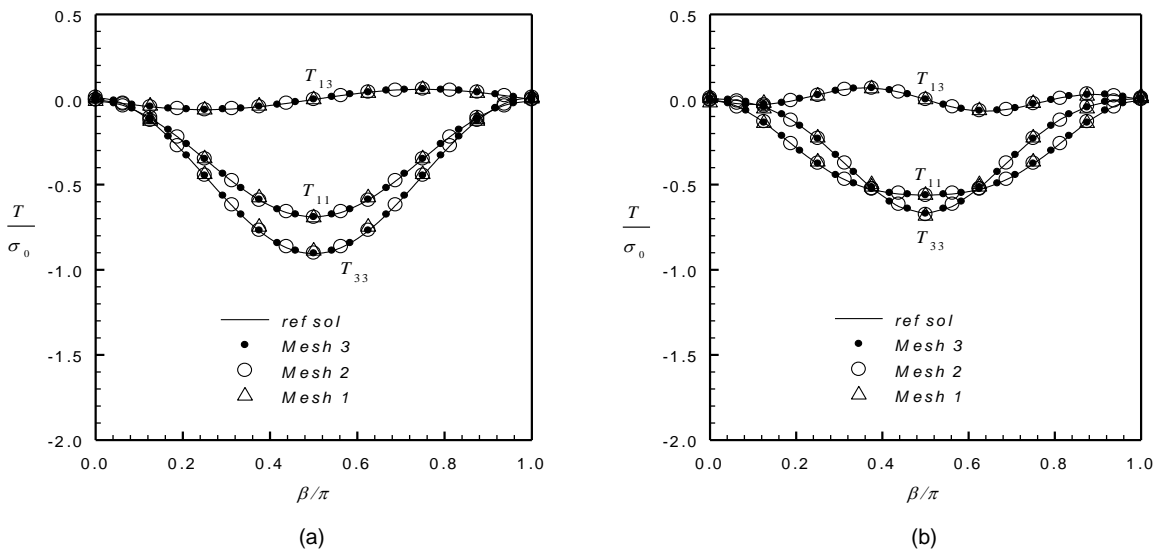


Fig. 11. Normalized T-stress components for vertical crack in whole space subjected to self-equilibrated, non-uniform normal traction $t_1^+ = t_3^+ = 0, t_2^+ = -\sigma_0(x_3/a)^2$ for (a) isotropic material and (b) transversely isotropic material.

and this therefore renders the technique more suitable for linear fracture analysis than the standard finite element method which generally requires sufficiently fine meshes to capture the near-front field and experiences difficulty in the treatment of an unbounded domain. While the proposed technique has been successfully implemented, it is still restricted to either a cracked whole-space possessing the plane of symmetry or a cracked half-space under symmetric boundary conditions. The potential extension of the current work to treat other types of boundary conditions such as the anti-symmetric,

traction-free and rigid boundary conditions and other types of materials such as multi-field and smart solids is considered essential. It is important to emphasize that besides the reduction of the computational cost directly gained from using the equivalent half-space model instead of the full treatment of a cracked whole space under a symmetric condition, the key ingredients and results established in the present study also form the useful and essential basis for further nontrivial generalization.

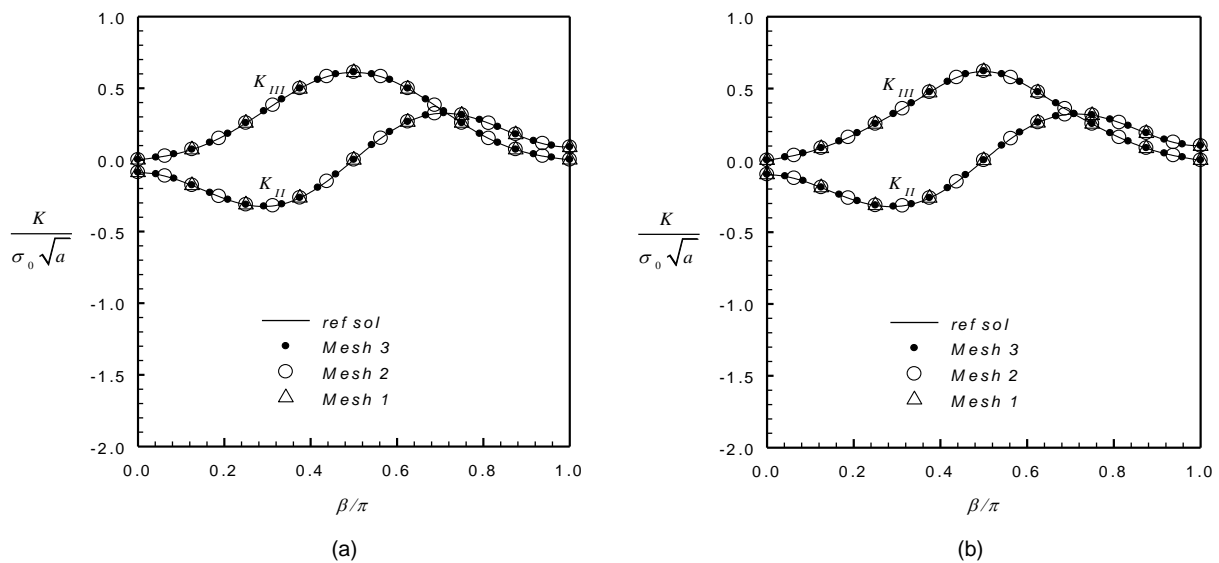


Fig. 12. Normalized mode-II and mode-III stress intensity factors for vertical crack in whole space subjected to self-equilibrated, non-uniform shear traction $t_2^+ = t_3^+ = 0, t_1^+ = \sigma_0(x_3/a)^2$ for (a) isotropic material and (b) transversely isotropic material.

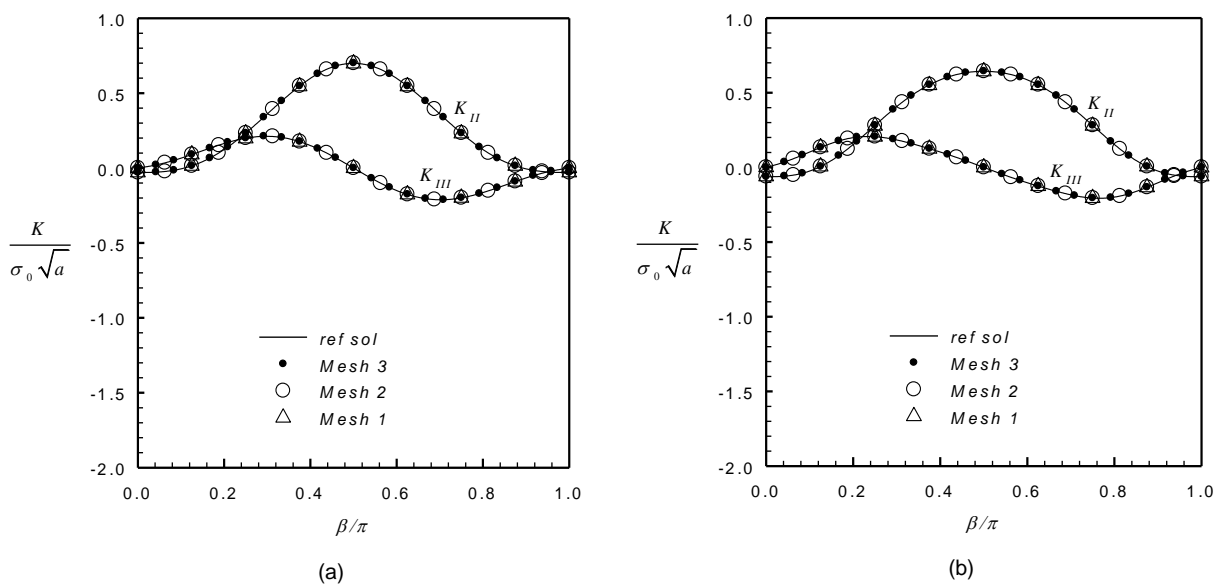


Fig. 13. Normalized mode-II and mode-III stress intensity factors for vertical crack in whole space subjected to self-equilibrated, non-uniform shear traction $t_1^+ = t_2^+ = 0, t_3^+ = \sigma_0(x_3/a)^2$ for (a) isotropic material and (b) transversely isotropic material.

Acknowledgements

The authors gratefully acknowledge the support provided by AUN/SEED-Net Program (JICA) and Thailand Research Fund (Grant No. RSA5980032).

References

- Ariza, M.P., Saez, A. and Dominguez, J., 1997. A singular element for three-dimensional fracture mechanics analysis. *Engineering Analysis with Boundary Elements*, **20**: 275-285.
- Ariza, M.P. and Dominguez, J., 2004. Boundary element formulation for 3D transversely isotropic cracked bodies. *International Journal for Numerical Methods in Engineering*, **60**: 719-753.
- Bonnet, M., 1995. Regularized direct and indirect symmetric variational BIE formulations for three-dimensional elasticity. *Engineering Analysis with Boundary Elements*, **15**: 93-102
- Bui, H.D., 1977. An integral equations method for solving the problem of a plane crack of arbitrary shape. *Journal of the Mechanics and Physics of Solids*, **25**(1): 29-39.
- Chen, W.Q. and Shioya, T., 2000. Complete and exact solutions of a penny-shaped crack in a piezoelectric solid: antisymmetric shear loadings. *International Journal of Solids and Structures*, **37**: 2603-2619.
- Chen, M.C., 2003a. Application of finite-part integrals to the three-dimensional fracture problems for piezoelectric media, Part I: hypersingular integral equation and theoretical analysis. *International Journal of Fracture*, **121**: 133-148.
- Chen, M.C., 2003b. Application of finite-part integrals to the three-dimensional fracture problems for piezoelectric media, Part II: numerical analysis. *International Journal of Fracture*, **121**: 149-161.
- Frangi, A., Novati, G. and Springhetti, R., 2002. 3D fracture analysis by the symmetric Galerkin BEM. *Computational Mechanics*, **28**: 220-232.
- Gray, L.J., Martha, L.F. and Ingraffea, A.R., 1990. Hypersingular integrals in boundary element fracture analysis. *International Journal for Numerical Methods in Engineering*, **29**: 1135-1158.
- Gu, H. and Yew, C.H., 1988. Finite element solution of a boundary integral equation for mode-I embedded three-dimensional fractures. *International Journal for Numerical Methods in Engineering*, **26**: 1525-1540.
- Li, S., Mear, M.E. and Xiao, L., 1998. Symmetric weak-form integral equation method for three-dimensional fracture analysis. *Computer Methods in Applied Mechanics and Engineering*, **151**: 435-459.
- Martha, L.F., Gray, L.J. and Ingraffea, A.R., 1992. Three-dimensional fracture simulation with a single-domain, direct boundary element formulation. *International Journal for Numerical Methods in Engineering*, **35**: 1907-1921.
- Martha, L.F., Wawrzynek, P.A. and Ingraffea, A.R., 1993. Arbitrary crack representation using solid modeling. *Engineering with Computers*, **9**: 63-82.
- Martin, P.A. and Rizzo, F.J., 1996. Hypersingular integrals: how smooth must the density be? *International Journal for Numerical Methods in Engineering*, **39**: 687-704.
- Mendelsohn, D.A., 1984a. A review of hydraulic fracture modeling-part I: general concepts, 2D models, motivation for 3D modeling. *Journal of Energy Resources Technology*, **106**: 369-376.
- Mendelsohn, D.A., 1984b. A review of hydraulic fracture modeling-part II: 3D modeling and vertical growth in layered rock. *Journal of Energy Resources Technology*, **106**: 543-553.
- Qin, T. and Noda, N.A., 2004. Application of hypersingular integral equation method to a three-dimensional crack in piezoelectric materials. *JSME International Journal*, **47**(2): 173-180.
- Rungamornrat, J. and Wheeler, M.F., 2006. Weakly-singular integral equations for Darcy's flow in anisotropic porous media. *Engineering Analysis with Boundary Elements*, **30**(4): 237-246.
- Rungamornrat, J., 2006. Analysis of 3D cracks in anisotropic multi-material domain with weakly singular SGBEM. *Engineering Analysis with Boundary Elements*, **30**(10): 834-846.
- Rungamornrat, J. and Mear, M.E., 2008a. Weakly-singular, weak-form integral equations for cracks in three-dimensional anisotropic media. *International Journal of Solids and Structures*, **45**: 1283-1301.
- Rungamornrat, J. and Mear, M.E., 2008b. A weakly-singular SGBEM for analysis of cracks in 3D anisotropic media. *Computer Methods in Applied Mechanics and Engineering*, **197**: 4319-4332.
- Rungamornrat, J., Phongtinnaboot, W. and Wijeyewickrema, A.C., 2015. Analysis of cracks in 3D piezoelectric media with various electrical boundary conditions. *International Journal of Fracture*, **192**: 133-153.
- Rungamornrat, J., Sukulthanasorn, N., Mear, M.E. Analysis for T-stress of Cracks in 3D Anisotropic Elastic Media by Weakly Singular Integral Equation Method. *Computer Methods in Applied Mechanics and Engineering* (under review)
- Saez, A., Ariza, M.P. and Dominguez, J., 1997. Three-dimensional fracture analysis in transversely isotropic

- solids. *Engineering Analysis with Boundary Elements*, **20**: 287-298.
- Sladek, V. and Sladek, J., 1982. Three dimensional crack analysis for an anisotropic body. *Applied Mathematical Modeling*, **6**(5): 374-380.
- Srivastava, K.N. and Singh, K., 1969. The effect of penny-shaped crack on the distribution of stress in a semi-infinite solid. *International Journal of Engineering Science*, **7**: 469-490.
- Swenson, D.V. and Ingraffea, A.R., 1988. Modeling mixed-mode dynamic crack propagation using finite elements: theory and applications. *Computational Mechanics*, **3**: 381-397.
- Ting, T.C.T. and Lee, V.G., 1997. The three-dimensional elastostatic Green's function for general anisotropic linear elastic solids. *The Quarterly Journal of Mechanics and Applied Mathematics*, **50**: 407-426.
- Wang, C.Y., 1997. Elastic fields produced by a point source in solids of general anisotropy. *Journal of Engineering Mathematics*, **32**: 41-52.
- Wang, X., 2004. Elastic T-stress solutions for penny-shaped cracks under tension and bending. *Engineering Fracture Mechanics*, **71**, 2283-2298.
- Weaver, J., 1977. Three-dimensional crack analysis. *International Journal of Solids and Structures*, **13**: 321-330.
- Xu, G. and Ortiz, M., 1993. A variational boundary integral method for the analysis of 3-D cracks of arbitrary geometry modelled as continuous distributions of dislocation loops. *International Journal for Numerical Methods in Engineering*, **36**: 3675–3701.
- Xu, G., 2000. A variational boundary integral method for the analysis of three-dimensional cracks of arbitrary geometry in anisotropic elastic solids. *Journal of Applied Mechanics*, **67**: 403–408
- Zhao, M.H., Fang, P.Z, and Shen, Y.P., 2004. Boundary integral-differential equations and boundary element method for interfacial cracks in three-dimensional piezoelectric media. *Eng. Analysis with Boundary Elements*, **28**: 753-762.
- Brebbia, C.A. and Dominguez, J., 1989. *Boundary elements: an introductory course*. McGraw-Hill Publishing, New York, Second Eds.: pp 293.
- Cruse, T.A., 1988. *Boundary element analysis in computational fracture mechanics*. Kluwer Academic Publishers Publishing, Dordrecht, The Netherlands: pp 171.
- Hughes, T.J.R., 2000. *The finite element method: linear static and dynamic finite element analysis*. Dover Publishing, Mineola, New York: pp 704.
- Liggett, J.A. and Liu, L.F., 1983. *The boundary integral equation method for porous media flow*. Allen and Unwin publishing, London: pp 255.
- Oden, J.T. and Carey, G.F., 1984. *Finite elements: special problems in solid mechanics*, Vol. 5. Prentice-Hall Publishing, Englewood Cliffs, New Jersey: pp 273.
- Yew, C.H., 1997. *Mechanics of Hydraulic Fracturing*. Gulf Publishing Company Publishing, Houston, Texas, First Ed.: pp 182.
- Zienkiewicz, O.C. and Taylor, R.L., 2000. *The finite element method: solid mechanics*, Vol. 2. Butterworth-Heinemann Publishing, Linacre House, Jordan Hill, Oxford, Fifth Eds.: pp 459.
- Ayhan, A.O., Kaya, A.C., Laflen, J., McClain, R.D. and Slavik, D., 2003. *Fracture analysis of cracks in orthotropic materials using ANSYS*. Reports No. GRC370, GEGlobal Research, General Electric Company (unpublished).
- Li, S., 1996. *Singularity-reduced integral equations for discontinuities in three dimensional elastic media*. Ph.D. Thesis, The University of Texas at Austin, Texas (unpublished).
- Pham, T.N., 2015. *Analysis of cracks in transversely isotropic, linear elastic half-space by weakly singular boundary integral equation method*. Ph.D. Thesis, Chulalongkorn University, Thailand, (unpublished).
- Xiao, L., 1998. *Symmetric weak-form integral equation method for three dimensional fracture analysis*. Ph.D. Thesis, The University of Texas at Austin, Texas (unpublished).
- Mayrhofer, K. and Fischer, F.D., 1989. *Stress intensity factor variation of a penny-shaped crack situated close to the free surface of a half-space*. In: Salama K, Taplin DMR, Rama Rao P, Ravi-Chandar K, editors. *Advances in fracture research. Proceedings of the 7th International Conference on Fracture (ICF7)*, March 20-24, 1989, Houston, Texas: 83-89.

Symbols and abbreviations

| | |
|--|--|
| a | Crack radius |
| BIEM | Boundary integral equation method |
| \mathbf{a}, \mathbf{b} | Orthonormal vectors |
| C_{mj}^{ik}, G_{mj}^p | Weakly singular kernels for whole space |
| $\bar{C}_{mj}^{ik}, \bar{G}_{mj}^p$ | Weakly singular kernels for whole space under symmetric conditions |
| $D_m(\cdot)$ | Surface differential operator |
| E_{ijkl} | Global components of elastic moduli |
| \bar{E}_{ijkl} | Local components of elastic moduli |
| $\mathbf{e}_1, \mathbf{e}_2, \mathbf{e}_3$ | Orthonormal base vectors of global Cartesian coordinate system |

| | | | |
|-----------------------------------|---|--|--|
| $\bar{e}_1, \bar{e}_2, \bar{e}_3$ | Orthonormal base vectors of local Cartesian coordinate system | x | Source point |
| FEM | Finite element method | $\{x_c; \bar{x}_1, \bar{x}_2, \bar{x}_3\}$ | Local Cartesian coordinate system at x_c |
| H_{mj}^p | Singular function of $\mathcal{O}(1/r^2)$ | \bar{x} | Image point of source point x |
| \bar{H}_{mj}^p | Singular function of $\mathcal{O}(1/r^2)$ | z | Unit vector |
| K_I, K_{II}, K_{III} | Mode-I, Mode-II, Mode-III stress intensity factors | $\delta(\xi - x)$ | Dirac-delta distribution centered at x |
| n^+, n^- | Outward unit normal vectors to crack surfaces | δ_{ij} | Standard Kronecker-delta symbol |
| $\{O; x_1, x_2, x_3\}$ | Global Cartesian coordinate system | $\bar{\delta}_{ij}$ | Modified Kronecker-delta symbol |
| r | Distance between source and field points | ε_{ijk} | Standard alternating symbol |
| S_c^+, S_c^- | Geometrically identical crack surfaces | $\bar{\varepsilon}_{ij}$ | Local components of finite part of strain tensor |
| S_{ij}^p | Stress fundamental solution for whole space | (ξ, η) | Master coordinates of point within the crack-tip element |
| T_{ij} | T-stress tensor | ξ | Field point |
| t_j^+, t_j^- | Tractions applied to crack surfaces | $\bar{\xi}$ | Image point of field point ξ |
| \tilde{t}_p, \tilde{u}_p | Test functions | σ | Stress field |
| U_j^p | Displacement fundamental solution for whole space | Σ_{ij}^{lk} | Hyper singular kernel of whole space |
| u | Displacement field | Ω | Cracked whole space under symmetric condition |